LETTER • OPEN ACCESS

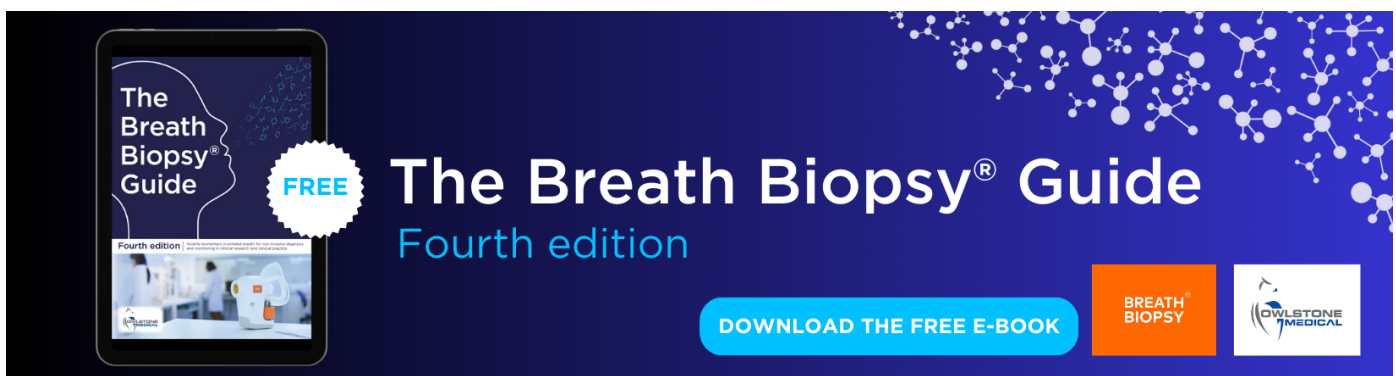# Characterization and process understanding of tropical cyclone-induced floods derived from observations in Shenzhen, China

View the article online for updates and enhancements.

ENVIRONMENTAL RESEARCH
LETTERS

LETTER

Characterization and process understanding of tropical cyclone-induced floods derived from observations in Shenzhen, China

Jingru Liu[1,2], Zhan Tian[2,*], Steven Dobbie[1], Andrew N Ross[1] , Laixiang Sun[3] and Qinghua Ye[4]

1   School of Earth and Environment, University of Leeds, Leeds LS2 9JT, United Kingdom
2   School of Environmental Science and Engineering, Southern University of Science and Technology, Shenzhen 518055, People's Republic of China
3   Department of Geographical Sciences, University of Maryland, College Park, MD 20742, United States of America
4   Deltares, Delft, The Netherlands
*   Author to whom any correspondence should be addressed.

E-mail: tianz@sustech.edu.cn

Abstract

Coastal cities like Shenzhen are confronting escalating flood risks under the combined impact of climate change and rapid urbanization, especially the tropical cyclones (TC)-induced flood. Incorporating the impact of climate change and urbanization on the flood, this study constructed a new TC-induced flood model on western Shenzhen embedded with a unique statistical approach. Based on extensive historical data and machine learning techniques, the temporal characteristics and changes of flooding were revealed. The results reveal an increase in the frequency of TC-induced floods between 1964–2022, especially after the 1990s, which is attributed to a decrease in the distance of the location of the maximum intensity of TCs (observed within an 800 km range of the study area) relative to the land, averaging a reduction of 11.4 km per decade. This shift towards land is likely due to changes in the locations of TC genesis. Furthermore, the 'rainfall sea level' threshold for western Shenzhen was accordingly derived from the results of modelling, which would enable decision-makers to quickly assess TC-induced flood risks. The study's proposed methods offer alternative approaches for predicting TC-induced floods in regions where the gathering of hydro-meteorological data is challenging or where economic and technological resources are limited.

1. Introduction

Coastal regions have historically been hubs of civilization, trade, and culture. However, they are also at the forefront of the challenges brought by climate change. Within a 100 km radius of coastlines, there are about 38% of the global population living in this region and 80% of flood-related fatalities worldwide between 1975 and 2016 occurred as well (Barbier 2015, Hu *et al* 2018). Coastal cities are more vulnerable to extreme hydrometeorological events (IPCC 2021). Floods induced by tropical cyclones (TC) are of particular concern that the accompanying intense storms and storm surges always have catastrophic effects on the living and production of the urban. The

combined impacts of sea level rise, land subsidence, and rapid urbanization would exacerbate these effects and lead to unprecedented socioeconomic loss (Liu *et al* 2022).

Located on the coast of the South China Sea, Shenzhen, a typical coastal megacity, epitomizes the challenges faced by coastal regions globally. Since its establishment in 1979, Shenzhen has undergone urbanization at an unprecedented pace. In 40 years, its built-up area has expanded 35 times, growing from 27 km^2 in 1979–946 km^2 in 2017 (Yu *et al* 2019). This rapid urbanization has brought about transformative land-use changes that may intensify the flood risks coupled with the rise of sea levels. In recent years, Shenzhen has experienced multiple

severe floods triggered by TCs. On 2nd and 8th September 2023, Super Typhoon Saola and Typhoon Haikui, hit the city in quick succession within a week and triggered shutdowns. The downpours brought by Typhoon Haikui broke seven historical records of the city since 1952. These records include the maximum rainfall over 2 h (195.8 mm), 3 h (246.8 mm), 6 h (349.7 mm), 12 h (465.5 mm), 24 h (557.8 mm), 48 h (613.8 mm), and 72 h (614.6 mm), causing massive flooding to Shenzhen (Xinhua 2023). Earlier super typhoons, Hato and Mangkhut in 2017 and 2018, had similarly devastating effects, highlighting the urgent need for effective TC-flood forecasting (Shenzhen Climate Bulletin 2018).

In response, the local government departments in Shenzhen have conducted a rigorous assessment of urban flood thresholds based on historical disaster data, survey insights, and other pertinent sources. This widely adopted assessment has informed the creation of a comprehensive table, enabled the estimation of specific rainfall thresholds at the subdistrict scale, and facilitated the evaluation of flood probabilities (Risk Warning for Major Meteorological Hazards in Shenzhen 2022). Machine learning (ML) has recently advanced urban flood forecasting, with studies like Zhang *et al* (2023), Ke *et al* (2020) applying ML algorithms to develop models for Shenzhen. However, these studies predominantly relied on rainfall data as the only input variable, potentially ignoring the complexity of TCs-induced floods.

Hydrological models are reliable tools for TC-induced flood study, offering robust support for a deeper understanding and prediction of flood events. However, most of the previous studies primarily focused on individual TC flood events, with a relative lack of research on long-term variations and trends of TC floods (Lee *et al* 2020, Yang *et al* 2021). In recent years, some researchers have indeed begun exploring this field (Joyce *et al* 2017, Zhang and Najafi 2020), Qiang *et al* (2021) also employed the SWMM model to simulate flood maps for the western coastal areas of Shenzhen under various combinations of rainfall and storm surges. Regrettably, these studies mainly concentrated on the long-term assessments of the impacts of sea-level rise on flooding, overlooking the potential effects brought about by urbanization. Moreover, as pointed out by Marsooli *et al* (2019), unlike simulations for rainfall-induced flooding events, TC-induced study needs to consider the variations in TC characteristics affected by climate change, an aspect that remains inadequately studied. As the establishment and operation of hydrological models often demand substantial computational resources and workforce, especially in acquiring high-quality hydro-meteorological and geographical data for studying flooding scenarios in larger regions, the application of hydrological models on urban floods is therefore limited.

Considering the aforementioned issues and challenges, the objectives of this study are to: (1) develop a TC-induced flood forecasting model that combines machine learning techniques with statistical approaches; (2) identify and analyse historical potential TC-induced flood events in Shenzhen, examine changes in their frequency and discern possible natural causes.

2. Study area & data sources

Shenzhen, a coastal metropolis, is located in the south of Guangdong Province, China, with a geographic location between 113°43′–114°38′ E and 22°24′–22°52′ N. The city borders the Pearl River Estuary to the west and Hong Kong to the south (figure 1). There are around five TCs affecting Shenzhen on average every year. This study narrows down to the western portion due to the long-term sea level observations available at the ChiWan site, representing Shenzhen's western sea area. Focusing on four out of nine river basins that flow into this area, namely Maozhou River, Pearl River Estuary, Shenzhen Bay, and Shenzhen River basins, this region holds hydrological significance and embodies Shenzhen's core urban zones, marked as the most vulnerable in Shenzhen by prior research (Sarica *et al* 2021).

The observational 24-h rainfall data (00:00–24:00 UTC) and daily maximum sea level data (astronomical surge + storm surge) are collected from the Shenzhen Hydrological Yearbook (1964–2019) and Shenzhen Meteorological Bureau (2020–2022). The locations of the stations are shown in figure 1(b). Given the lack of data on storm surges in Shenzhen, the dates of maximum storm surges and sea levels of Hong Kong (North Point/Quarry Bay station) are used here, which are obtained from Tropical Cyclone Yearbook provided by Hong Kong Observatory and Chan (1983). Historical TC flood disaster information (2001–2022) is provided by the Shenzhen Meteorological Bureau and the Shenzhen Water Affairs Bureau. Additionally, records of seven TC-induced flood events (IDA, 1964; RUBY, 1964; ELLEN, 1983; GORDON, 1989; BECKY, 1993; SAM, 1999; YORK, 1999) are from the Collection of Storm Surge Disasters Historical Data in China 1949–2009 (Yu *et al* 2015), Shenzhen flood control plan revision and river improvement plan: Revision report of flood control plan (2014–2020). The land-use data originate from the National Earth System Science Data Centre. The historical length of the drainage network data is collected from the official website of Shenzhen Water Authority and Peng *et al* (1999). The track and intensity data of TCs are obtained from the Western North Pacific tropical cyclone database (Ying *et al* 2014, Lu *et al* 2021). The monthly sea surface temperature (SST) data is from the Met Office Hadley Centre
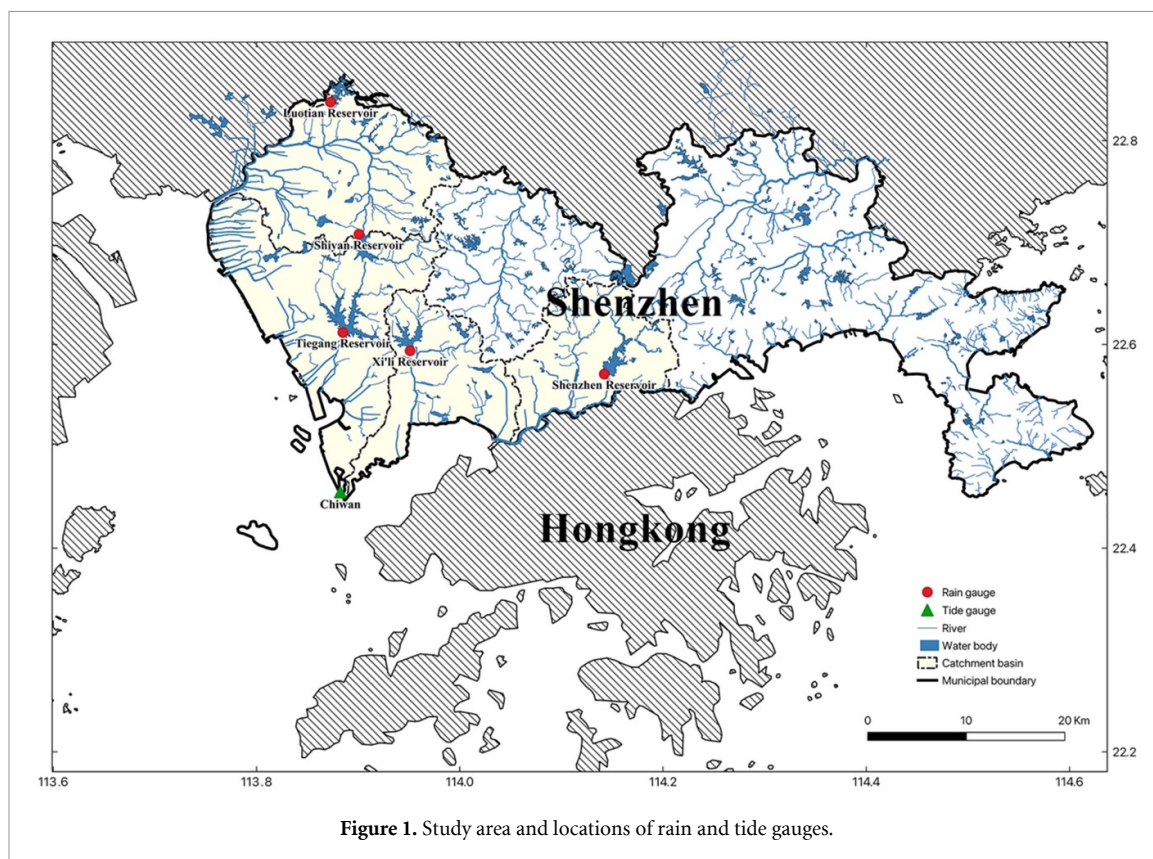
Figure 1. Study area and locations of rain and tide gauges.

SST dataset, and the monthly wind data is from the NCEP/NCAR (Reanalysis-1) dataset.

3. Methods

This study consists of four steps as shown in figure 2.

3.1. Input data pre-processing

3.1.1. Maximum sea level & maximum daily rainfall
The daily maximum rainfall and maximum sea level occurring within ± 1 d of the maximum storm surge event are collected. In total, 340 TCs are studied in this research. Note that the sea level data of Typhoon Viola (1964) in Shenzhen is missing, it is estimated by the fitting function of the remaining 339 TCs' sea level data at Shenzhen and Hong Kong (figure A1). The maximum sea level of Typhoon Viola (1964) in Shenzhen was calculated to be about 1.4 m. Detailed information can be found in the appendix.

3.1.2. Flood risk composite index (FRCI)
To address the potential influences of climate change and urbanization on flooding events over time, a FRCI is constructed. The process involves:

1. Establishment of Flood Sensitivity Factors: (1) Based on land-use data, the ratio of impervious area to green area (forest, grassland, farmland), and water area for each year in the study area were calculated (figure A2). Since Shenzhen was established in 1979, with minimal land-use changes before that, data from 1980 was used for the period between 1964 and 1979. (2) Historical drainage network length served as a measure of urban drainage capacity. Similarly, since the construction of Shenzhen's drainage system began in 1980 and was minimal before that (Chen 2014). (3) Accounting for the effects of sea-level rise and land subsidence, a relative sea-level rise measurement was constructed. The average rate of sea level rise near the study area is approximately 3.5 mm yr^{-1} (Zou *et al* 2021, Ministry of Natural Resources 2023), and the mean subsidence rate is about 2.5 mm yr^{-1} (Ma *et al* 2019, Wang *et al* 2012b). The sum of the two rates is 6 mm yr^{-1}, consistent with the findings of Nicholls *et al* (2021). However, the rate of land subsidence in Shenzhen before 1986 tended to be zero (Huang *et al* 2001), and considering that Shenzhen entered a period of rapid construction and development after 1990 (Ng 2003, Du 2020), the influence of urban construction on land subsidence gradually became apparent. Therefore, for the period from 1964 to 1990, only sea-level rise was considered as a factor, while both sea-level rise and ground subsidence were included from 1990 onwards.
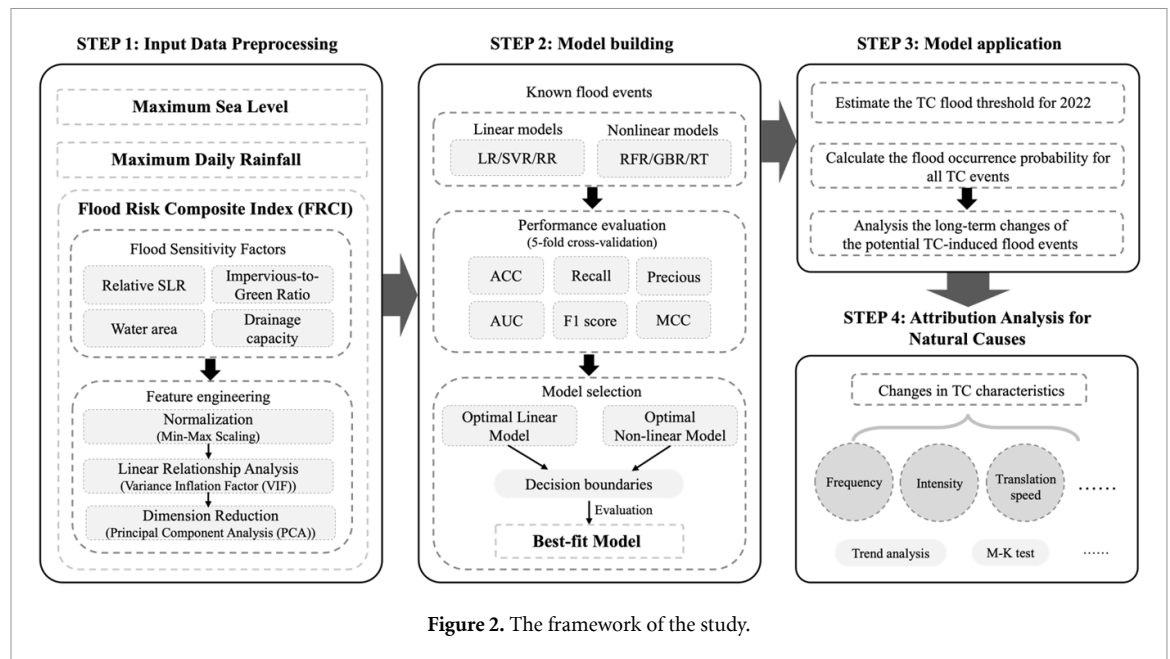
2. Normalization: To eliminate the influence of scales, Min-Max Scaling was applied to the four factors (figure A3).

3. Linear Relationship Analysis: To reduce redundancy among factors, the Variance Inflation Factor

Figure 2. The framework of the study.

(VIF) was utilized to assess the linear relationships between factors. It was found that the VIF values for 'Relative SLR,' 'Impervious-to-Green Ratio,' and 'Drainage capacity' are significantly greater than 10, indicating potential serious multicollinearity issues.

4. Dimensionality Reduction: principal component analysis was employed to reduce the dimensionality of these factors, and the first principal component, which explained approximately 91% of the variance (figure A4)), was selected as the FRCI as shown in figure A4).

3.2. Model building & application

Machine learning is used to extract the main features of massive data samples through algorithms, and make predictions according to the learned rules. The process of building a machine learning model includes structural construction of data, model building, and validation. Flood prediction is usually an application of binary classification (e.g. 'true and false', 'yes and no'), which aims to distinguish flood events from non-flood events based on hydrological variables (Ke *et al* 2020, Schmidt *et al* 2020, Chang *et al* 2022). However, this study aims to establish a model to predict the likelihood of flood occurrence, providing a continuous probability value instead of a binary classification.

Considering the limited sample size, several commonly used regression models were considered, encompassing both linear models (logistic regression (LR), support vector regression (SVR), and ridge regression (RR)) and nonlinear models (random forest regression (RFR), gradient boosting regression (GBR), and regression tree (RT)). To determine the optimal model, five-fold cross-validation was

employed, and the performance metrics of each model, including Accuracy, area under the curve (AUC), Recall, Precision, F1 Score and matthews correlation coefficient (MCC).

The decision boundary delineates the input feature space, providing insight into a model's decision-making process. By comparing these boundaries, the model that best captures the inherent data patterns is chosen for accurate flood predictions. Therefore, the decision boundaries of both optimal linear and non-linear models were analysed to select the best-fit model for this study. Finally, this three-dimensional best-fit model was used to estimate the TC flood threshold for 2022 and to calculate the probability of flooding for all TC events.

3.3. Attribution analysis methods

Standard linear regression and correlation analysis were employed in this study, and the significance levels are assessed using the standard two-tailed Student's t-test. In addition, the Mann–Kendall (M-K) test was used to test for abrupt changes. This method is widely applied to climate data and is highly effective in verifying a transition from a relatively stable state to another state (Xing *et al* 2018). More details about this method can be found in Mann (1945).
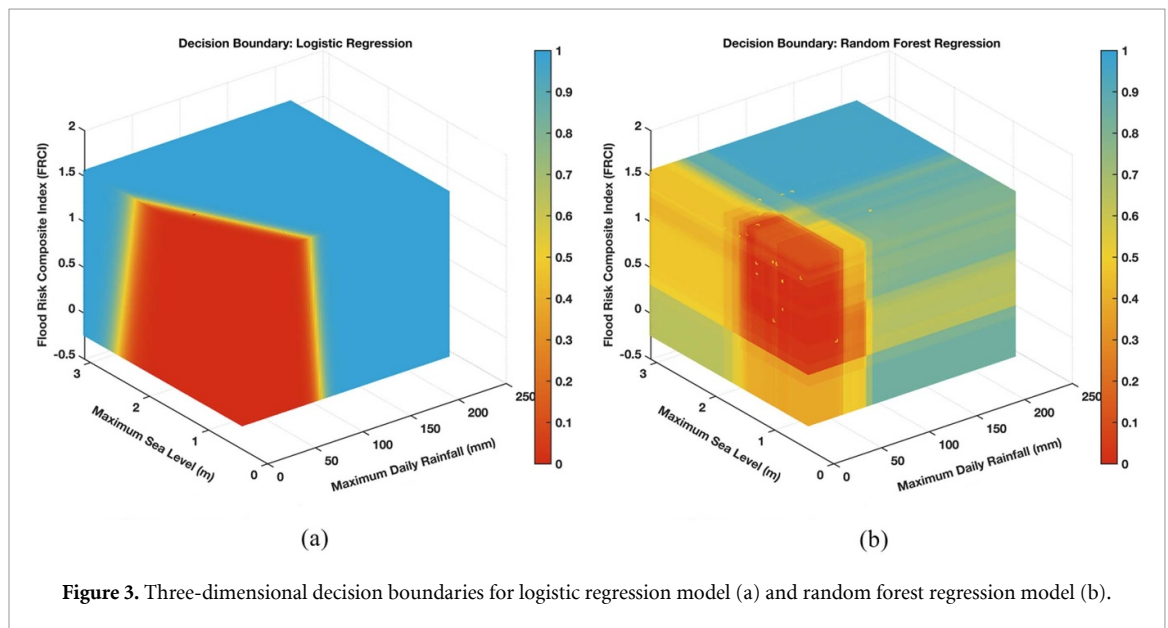
4. Results

4.1. Best-fit model for TC-induced flood prediction

The historic disaster information of 123 TCs was collected, with 51 experiencing floods and 72 not. Modelling was conducted on these TCs, with the target variable being the presence of floods, and the features including rainfall, sea level, and FRCI. The

Table 1. Performance metrics of machine learning models.

	Linear model			Nonlinear model		
	LR	SVR	RR	RFR	GBR	RT
Accuracy	0.92	0.84	0.85	0.89	0.89	0.89
AUC	0.98	0.97	0.98	0.96	0.94	0.95
Recall	0.92	0.61	0.65	0.84	0.86	0.86
Precision	0.89	1	1	0.90	0.86	0.86
F1 Score	0.90	0.76	0.78	0.87	0.86	0.86
MCC	0.83	0.69	0.72	0.78	0.77	0.77

Figure 3. Three-dimensional decision boundaries for logistic regression model (a) and random forest regression model (b).

results of the five-fold cross-validation for six ML models are shown in table 1. It can be observed that among the linear models, LR slightly lags behind SVR and RR in accuracy but performs the best in other metrics. Among the three non-linear models, RFR has slightly higher AUC and MCC compared to the others. In summary, LR is considered the top-performing linear model, while RFR is considered the top-performing non-linear model.

The decision boundaries of the LR and RFR models are illustrated in figure 3. The RFR model provides underestimated predictions for events featuring high sea levels and low rainfall. However, this discrepancy contradicts the reality that the topographic elevation remains constant in the study area. When the sea level exceeds the coastal elevation, flooding events are bound to occur even in the absence of rainfall. In comparison, the decision boundary provided by the LR model aligns more closely with reality and offers better interpretability. Therefore, the LR model is selected to be the best-fit model to predict TC-induced flood events.

4.2. TC-induced flood threshold for 2022

To determine the 'Rainfall-Sea level' flood threshold for western Shenzhen, the FRCI for the year 2022 was held constant. Subsequently, 10 000 sets of

data points, comprising rainfall and sea levels, were randomly generated. These data points were subjected to the established model to assess their respective flood risk levels, categorized as high, moderate, and low, as illustrated in figure 4.

To better align with practical emergency requirements and enhance the effectiveness of flood warnings, the decision boundary with a probability of 0.3 is taken as the TC-induced flood threshold for Shenzhen in the present. The threshold line can be presented as equation (1):

$$F(x) = -0.0265x + 2.2, \tag{1}$$

where x is the maximum daily rainfall.

4.3. Changes of TC-induced flood events and attribution analysis

Utilizing the established best-fit model, predictions were carried out for the entirety of the 59 year dataset encompassing all TC events. Consequently, the probability of flood occurrence for each TC event was computed. Subsequently, TC events with flood probabilities ⩾0.3 were identified as potential TC-induced flood events. 102 potential flooding events have been selected from the total of 340 TCs.

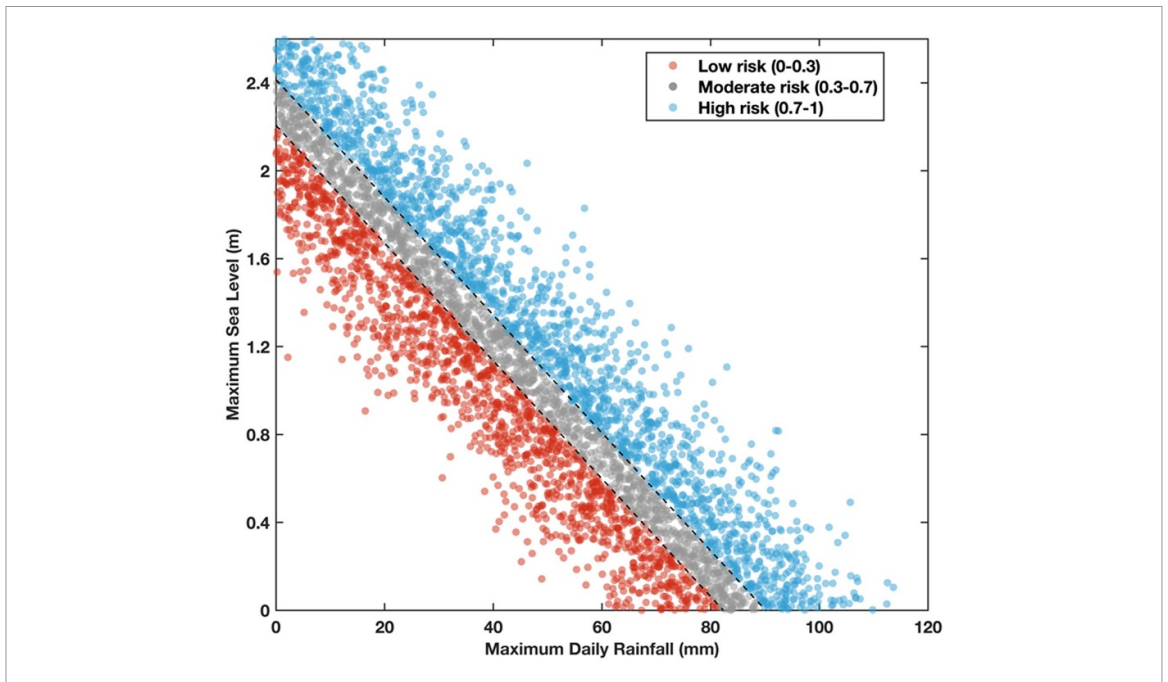Between 1964 and 2022, the frequency of potential TC-induced flooding events showed a significant

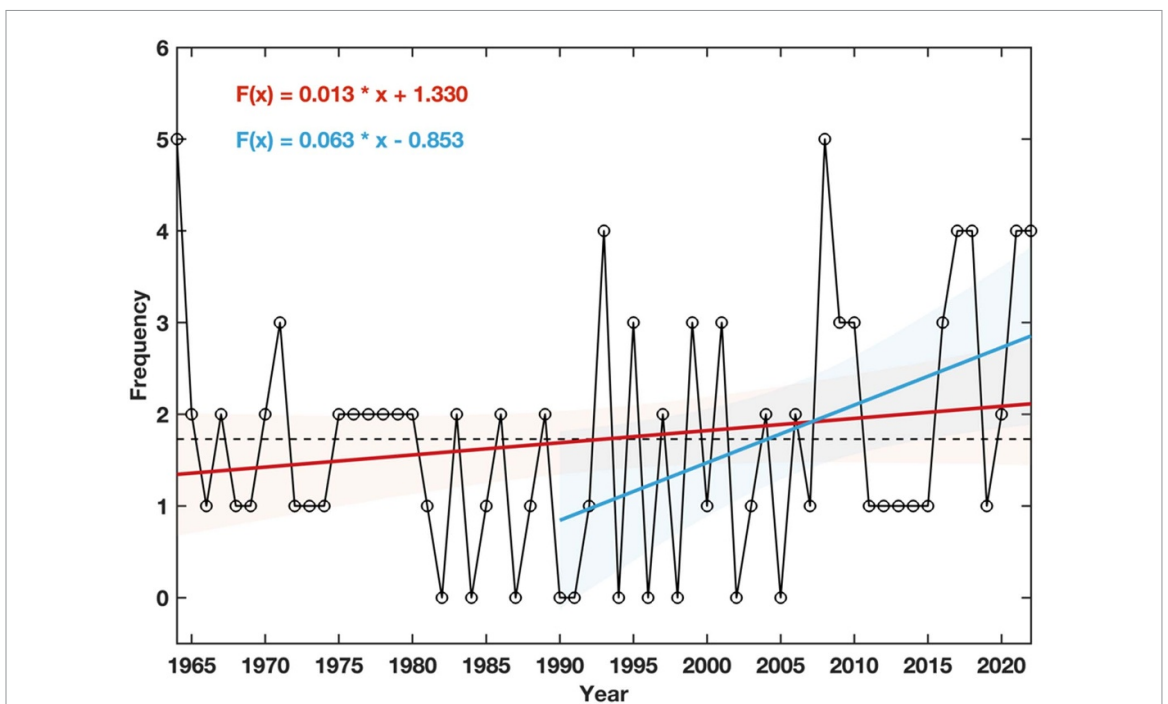**Figure 4.** Flooding threshold for 2022 derived from Logistic Regression model.

Figure 5. Frequency changes of the potential flood events. The dashed line represents the mean over the 59 years. Red and blue lines stand for the linear trends.

increasing trend (figure 5). In particular, it is obvious from the figure that the frequency of occurrence has been higher since the 1990s. However, during the same period, there is no statistically significant trend for TCs occurring in the south china sea (SCS), or coming within 800 km of the study area, or bringing storm surges to the region (figure A5). Therefore, the following sections consider possible reasons for this increasing trend.

Changes in TC characteristics can directly lead to changes in rainfall and storm surge, and thus affect the frequency of TC-induced flooding. Therefore, we conducted a series of statistical analyses for all 340 TCs during the 59 years. The results show that the time-series analysis of the number of TCs entering various distance ranges of the study area exhibits no discernible trend (figure A6), nor do changes in translational speed between 1964–2022, analysed both in
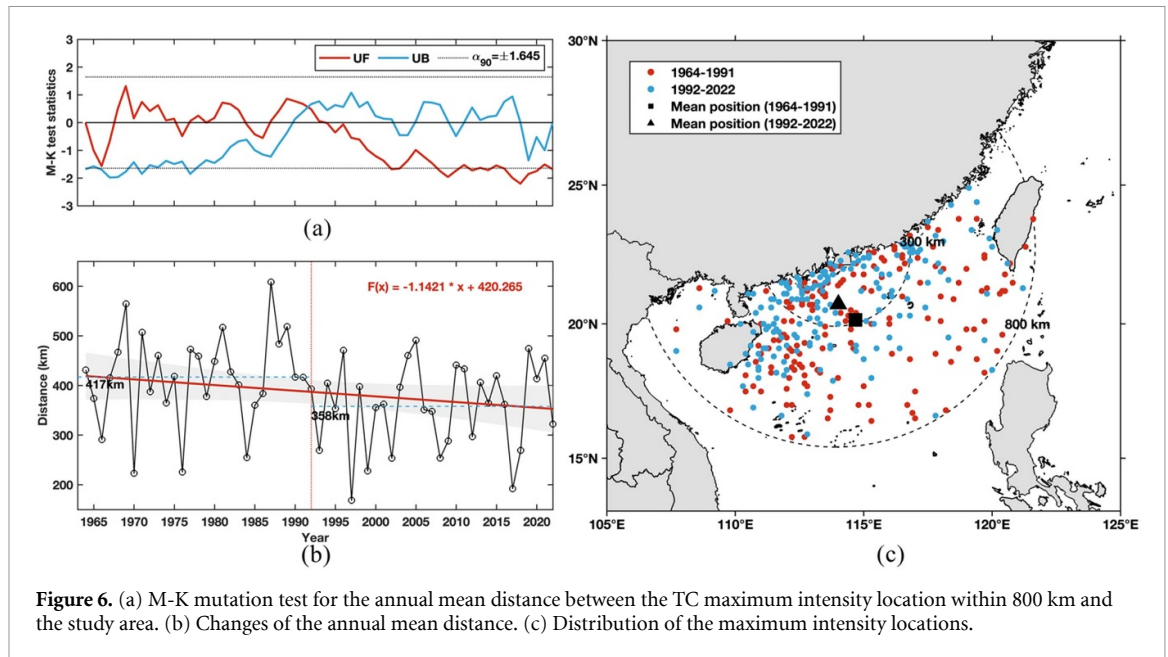
Figure 6. (a) M-K mutation test for the annual mean distance between the TC maximum intensity location within 800 km and the study area. (b) Changes of the annual mean distance. (c) Distribution of the maximum intensity locations.

terms of the mean overwater translation speed across different distance ranges of the study area and the translation speed pre and post-landfall (figures A7 and A8). Furthermore, a significant decrease at a 99.9% confidence level in the annual mean maximum intensity of TCs within 800 km during the period of 1964–2022 was observed (figures A9 and A10). It seems that none of these factors—the unchanged counts and translational speeds of TCs, along with the weakened intensity, lead to an increase in TC flooding events.

Observations indicate that TC motion has migrated coastward, poleward and westward due to tropical expansion as well as the higher relative SST along the coast (Daloz and Camargo 2017, Sun *et al* 2018, 2019, Knutson *et al* 2021, Wang and Toumi 2021). In this study, we found no significant change in the distribution of the closest locations to Shenzhen before TCs landed on the mainland (figure A11). However, the annual mean distance between the TC maximum intensity location and the study area decreases significantly (99.9% confidence level) at a rate of approximately 11.4 km per decade (figure 6(b)). The maximum intensity here refers to the maximum intensity within 800 km from the study area rather than the maximum intensity over the whole duration of the TC lifetime. To further analyse the trend changes of the annual mean distance, the M-K test method was implemented in this study (figure 6(a)). According to the intersection point position of the UF curve and the UB curve in figure 4(a), it can be inferred that the decrease in the distance appears to be a bifurcation point, which occurs around 1992. The annual mean distance between 1964–1991 is about 417 km, while that is about 358 km between 1992–2022, a difference of 59 km. Figure 4(c) shows the distribution of the

maximum intensity points in these two periods, the mean positions of the two periods are at 20.15° N, 114.68° E (triangle) and 20.72° N, 114.01° E (square), respectively, and the distance between them is about 94 km. Overall, the location of the maximum intensity of the TC is close to the Shenzhen/coast during 1964–2022, a finding that is consistent with the results derived by Wang and Toumi in 2022. These results suggest that the increased frequency of TC-induced floods is likely related to a decrease in the distance between the location of the TC maximum intensity and the land.

Wang and Toumi (2022) suggest that the primary driver of the shift in maximum intensity position could be the zonal changes in the environmental steering flow. However, in this study, there is no noticeable difference in the environmental steering flow near Shenzhen between the two periods (figure A12). We noticed significant differences in SSTs between the two periods, which are associated with the location of TC genesis. After comparison, we found that the TC genesis locations affecting Shenzhen were closer to the coast from 1992 to 2022, with a mean position that shifted north-westward by about 782 km compared to the mean genesis position during 1964–1991 (figure 7). In addition, the proportion of TC generated in the SCS; (0°–30° N, 106° E–120° E) increased from 21% to 34%. The identification of the SCS region here follows the partitioning methods previously reported (Song *et al* 2019, Wang *et al* 2012a). The observed north-westward migration of TC genesis locations may be associated with a 'La Niña-like' intensification of the zonal SST gradient across the equatorial Pacific. As detailed by Lee *et al* (2022), this La Niña-like/zonally asymmetric convection, is manifested in an enhanced SST gradient, a strengthened Walker circulation, and altered

Figure 7. Distribution of the genesis positions of TCs.
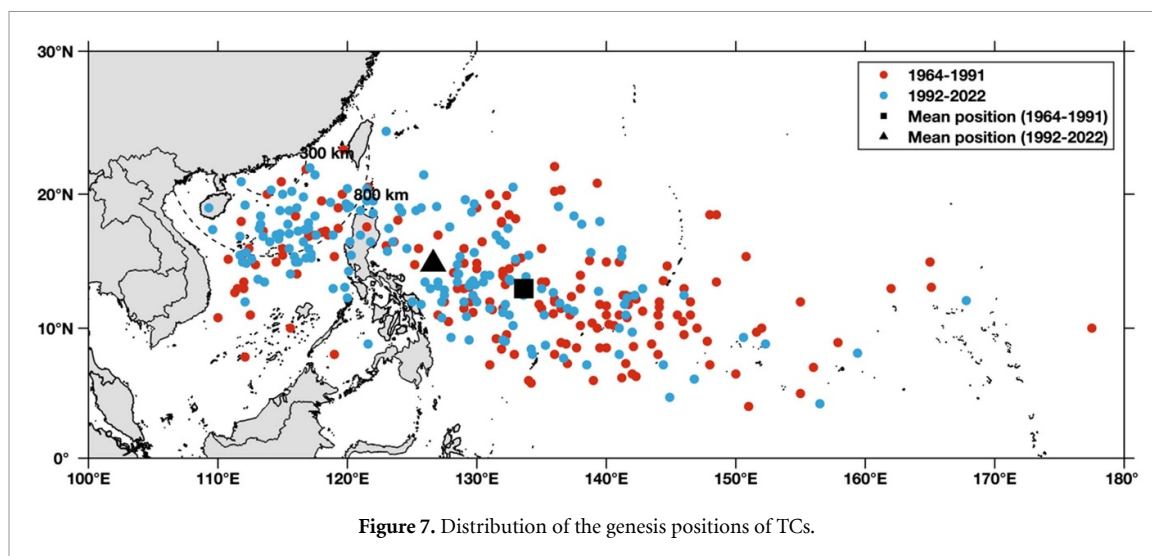
thermocline depths, culminating in warmer waters in the western Pacific. Consequently, this leads to the genesis of TCs further northwest, nearer to the Asian continent. Despite rising SSTs, TC genesis locations have shifted northwest without an increase in frequency (figure A5). Gao *et al* (2022) attribute this to subsurface ocean cooling in the tropical central-north Pacific during El Niño, which can modulate the ocean's response to atmospheric conditions, potentially offsetting the effects of sea surface warming on TC frequency. In conclusion, we believe that the decrease in the distance of TC maximum intensity to land in figure 6 may be mainly caused by the changes in the location of TC generation.

5. Conclusion & discussion

To summarise, this study employed statistical methods to predict flood events based on a rich, lengthy, decades-spanning historical dataset, combined with machine learning techniques, to delve deeper into the variations and characteristics of TC-induced flood events. The following conclusions have been drawn:

First, the LR model is the best-fit model to predict TC-induced flood events, utilizing rainfall, sea level, and flood risk composite index as characteristic variables. The model gives the current flood thresholds for Shenzhen. The threshold line was determined to be: $F(x) = -0.0265x + 2.2$. According to Nie *et al* (2016), when the sea level of Chiwan is higher than 1.4 m during a TC event, seawater intrusion will occur in western Shenzhen. However, the corresponding rainfall has not been mentioned in their research. Furthermore, Zhou *et al* (2017) reported that between 2012–2014, the maximum 24-hour precipitation of rainstorm-induced disasters in Shenzhen occurred in the range of 46–631 mm, which is mainly concentrated in the 100–300 mm range. Again, the effect of sea level was not considered in their study. The threshold of this study indicates that flooding may

occur if the sea level exceeds 2.2 m without precipitation, or if 24-hour rainfall exceeds 83 mm when the sea level is 0. Combined with the results of previous studies, it can be concluded that the calculated TC-induced flood threshold in our study has a higher degree of confidence than those in the literature. Indeed, the validation of our threshold still requires simulation through hydrological models or observational data from future TC events. In addition, the daily rainfall data does not adequately represent the intensity of rainfall during various times of the day. If the rainfall is gentle and within the capacity of the urban drainage system, the cumulative 24-hour rainfall can surpass the threshold line without causing flooding. Therefore, the intensity of TC-induced flooding needs to be further investigated in the future.

Second, the frequency of TC-induced floods was found to increase at an annual average rate of 1.3%, which is considered to be related to a decrease in the distance of TC maximum intensity, observed within an 800 km range of the study area, relative to the land. The location of the maximum intensity of the TC relative to the Shenzhen/coast decreased at a rate of approximately 11.4 km per decade, with an apparent bifurcation point in 1992. This shift is most likely due to the changes in the location of TC genesis, which is believed to be mainly driven by a 'La Niña-like' intensification of the zonal SST gradients across the equatorial Pacific under global warming. Since there was rapid urbanization that began in the 1990s, the increase in flood frequency may be due to urbanization effect enhancing TC rainfall or causing changes to urban hydrological processes. Additionally, the northward shift of the maximum intensity location could heighten storm surge and might also be influenced by urban land cover, which in turn could amplify precipitation. All these issues are planned to be investigated using numerical models in future work to provide a more comprehensive understanding and address the complex interactions between urbanization and TC-induced floods.

Despite the inherent uncertainties in models and data, flood predictions based on the 'rainfall-sea level' threshold derived by the machine learning approach in this study will enable decision-makers to quickly evaluate the flood risk associated with a TC within a short period. The findings of this study hold significant implications for Shenzhen's effective response to TC-induced flooding. Furthermore, the method of establishing the flood model in this paper provides a valuable approach for areas constrained by hydrological data acquisition or limited by economic and technological conditions.

Data availability statement

All data that support the findings of this study are included within the article (and any supplementary files).

Acknowledgments

Author contributions

T Z, L S and Q Y had the original idea and developed the conceptualization of the study. S D and A R helped frame the paper and provided guidance on the research methodology. J L conducted all data analyses and prepared the visualizations and the original draft of the manuscript. All co-authors contributed to the editing of the manuscript and to the discussion and interpretation of results.
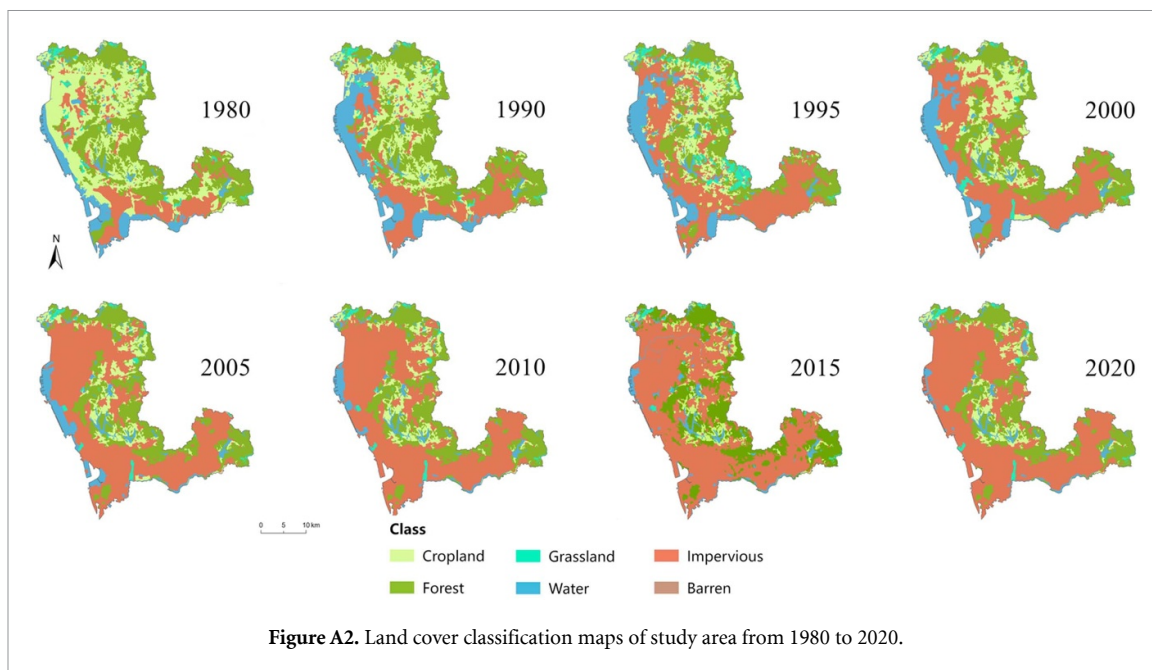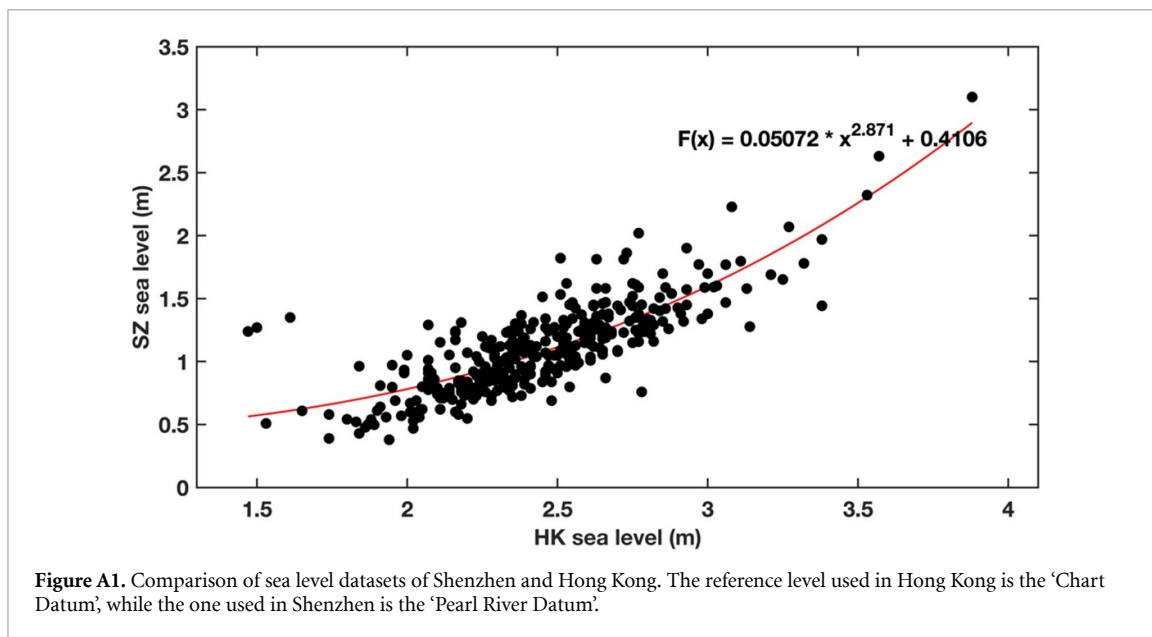
Conflict of interest

The contact author has declared that none of the authors has any competing interests.

Disclaimer

Publisher's note: Copernicus Publications remains neutral with regard to jurisdictional claims in published maps and institutional affiliations.
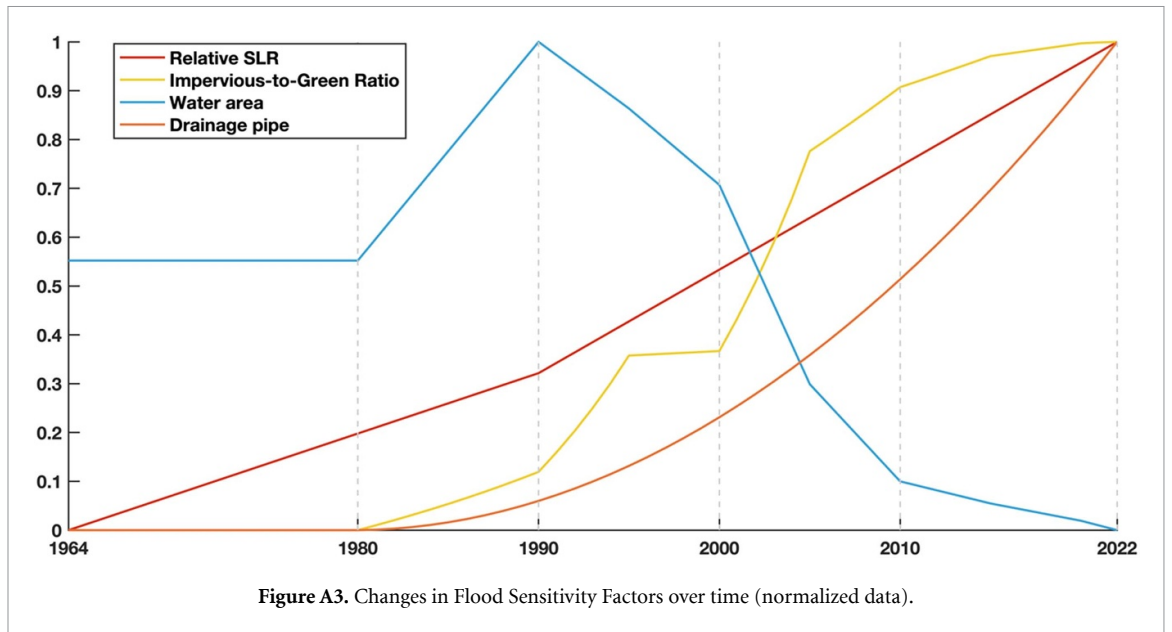
Appendix

Figure A1. Comparison of sea level datasets of Shenzhen and Hong Kong. The reference level used in Hong Kong is the 'Chart Datum', while the one used in Shenzhen is the 'Pearl River Datum'.

$$F(x) = 0.05072 * x^{2.871} + 0.4106$$

Figure A2. Land cover classification maps of study area from 1980 to 2020.

Figure A3. Changes in Flood Sensitivity Factors over time (normalized data).
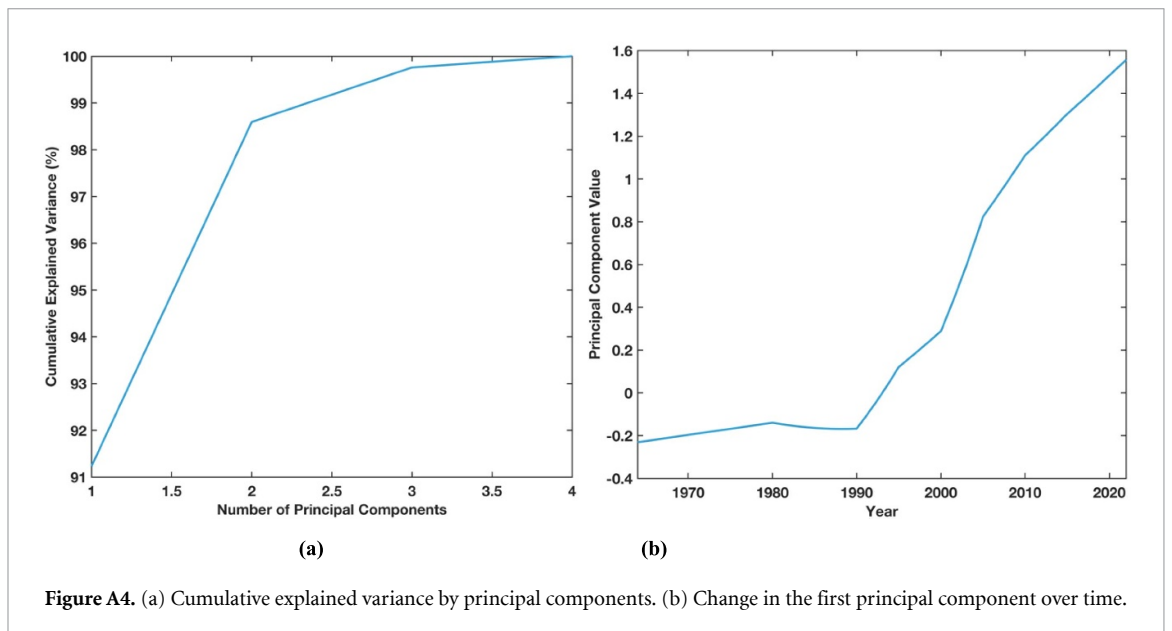

Figure A4. (a) Cumulative explained variance by principal components. (b) Change in the first principal component over time.
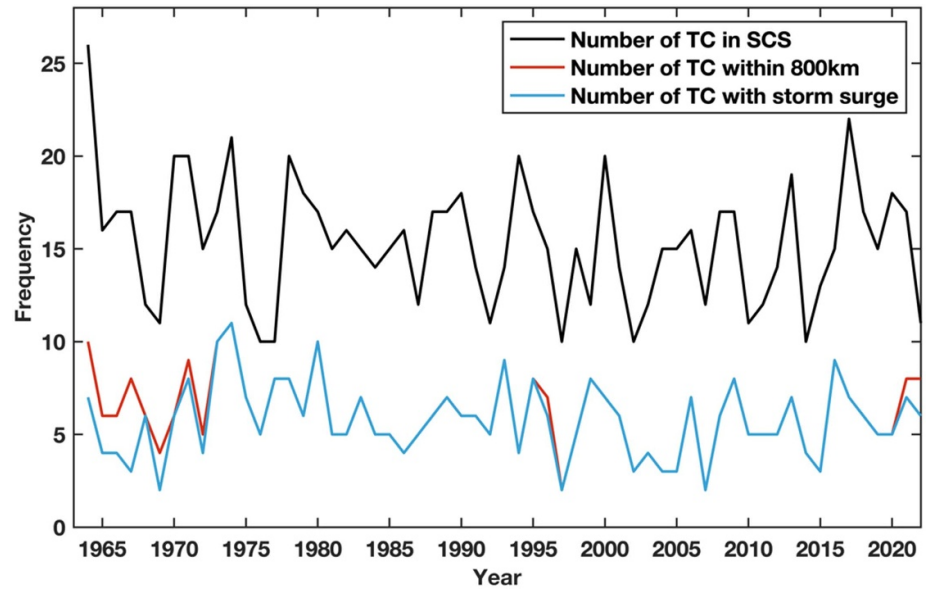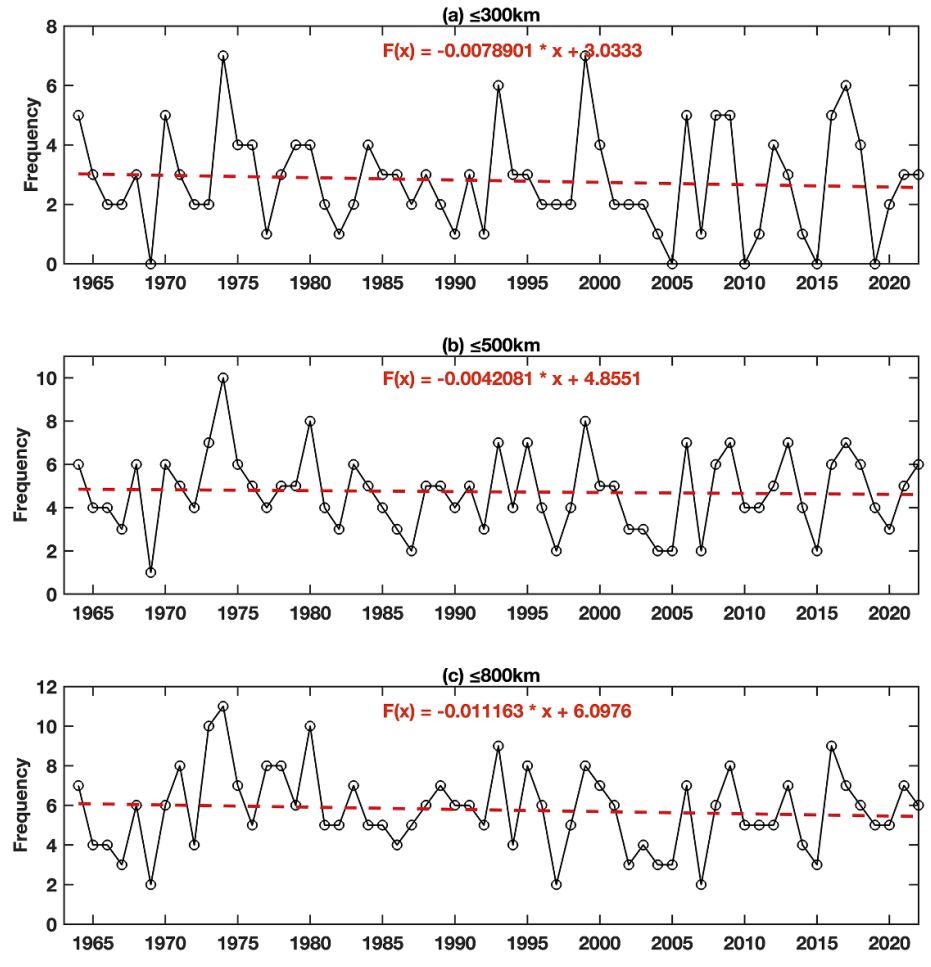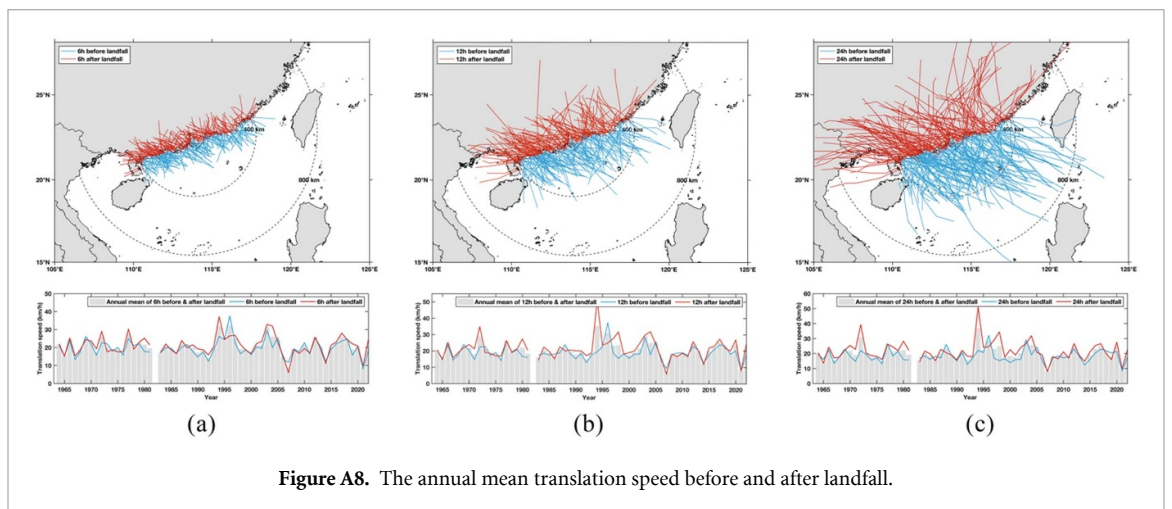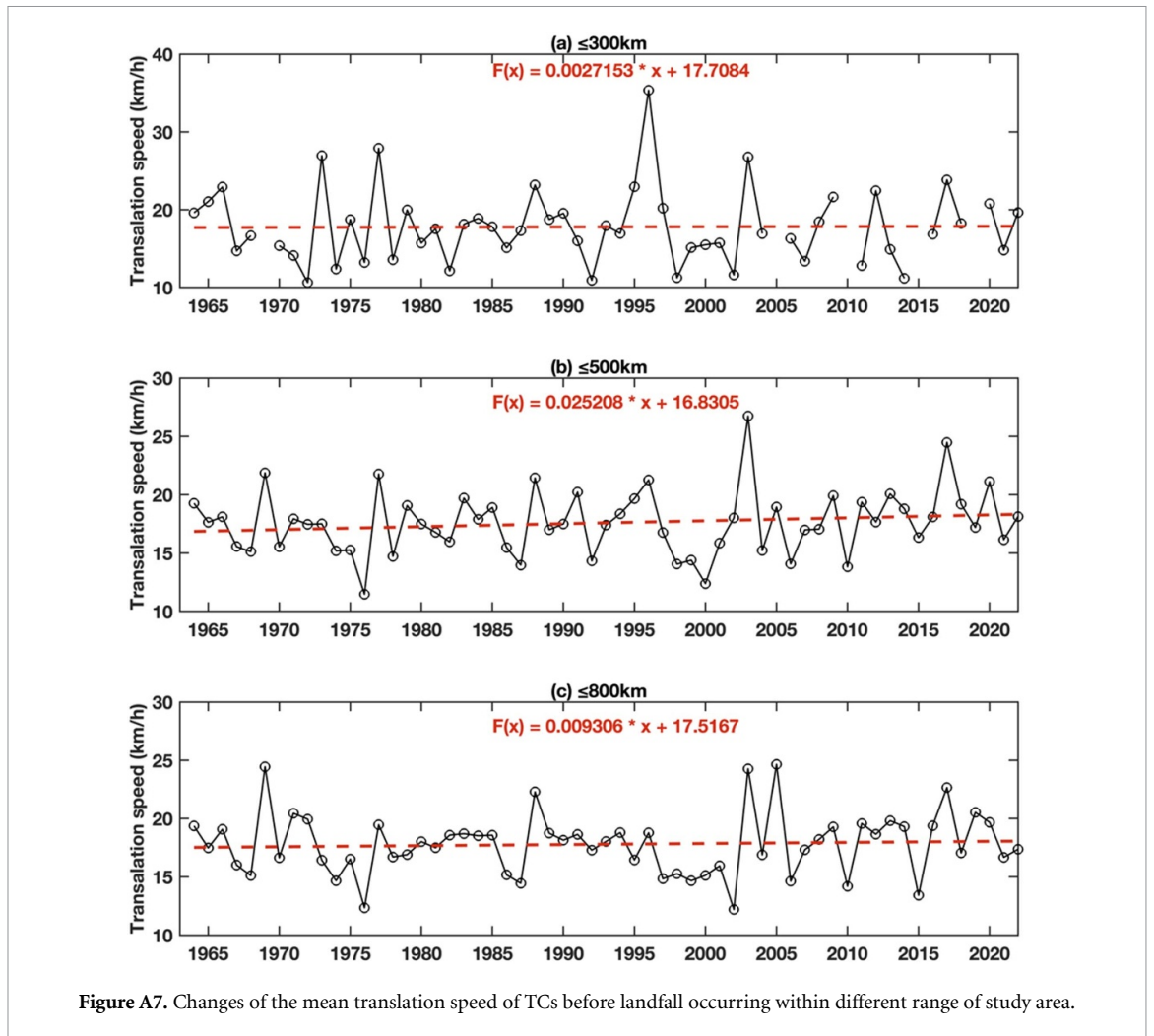
Figure A5. Frequency changes of TC events.

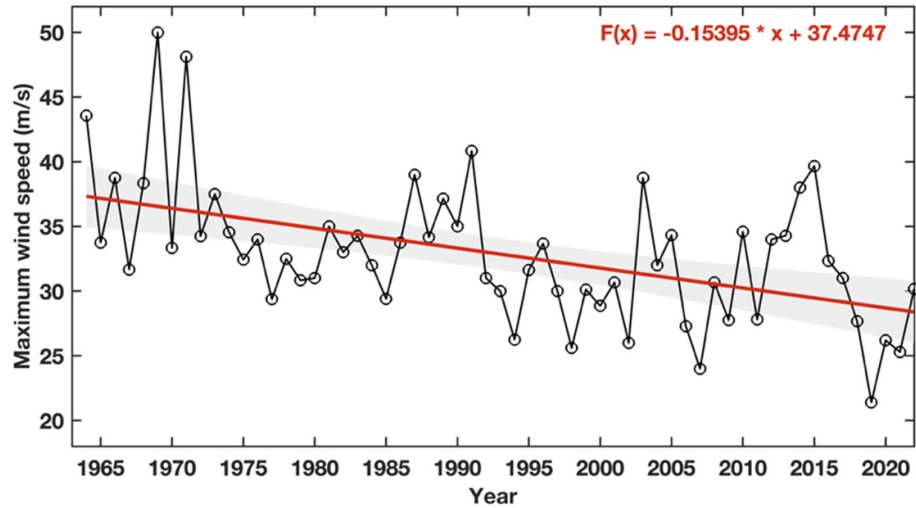**Figure A6.** Numbers of TCs in different ranges from the study area.

Figure A7. Changes of the mean translation speed of TCs before landfall occurring within different range of study area.

Figure A8. The annual mean translation speed before and after landfall.

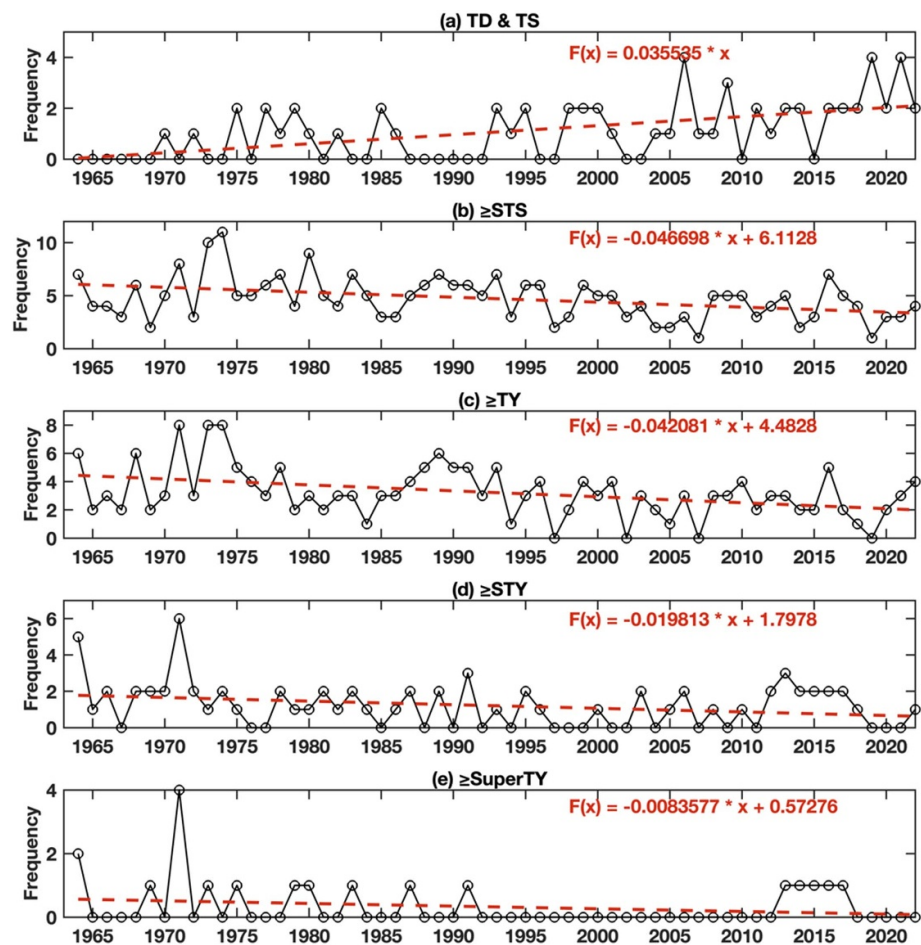**Figure A9.** The annual mean maximum intensity of TCs.

Figure A10. Frequency changes of different intensity categories' TCs occurring within 800 km of study area. (a) Tropical Depression (TD, 10.8–17.1 m s^{-1}) and Tropical Storm (TS,17.2–24.4 m s^{-1}); (b) ≥Severe Tropical Storm (STS, 24.5–32.6 m s^{-1}); (c) ≥Typhoon (TY, 32.7–41.4 m s^{-1}); (d) ≥Severe Typhoon (STY, 41.5–50.9 m s^{-1}); (e) ≥Super Typhoon (SuperTY, ≥51.0 m s^{-1}). The intensity categories used here are according to the Chinese National Standard for Grade of Tropical Cyclones (Ying *et al* 2014, Lu *et al* 2021).
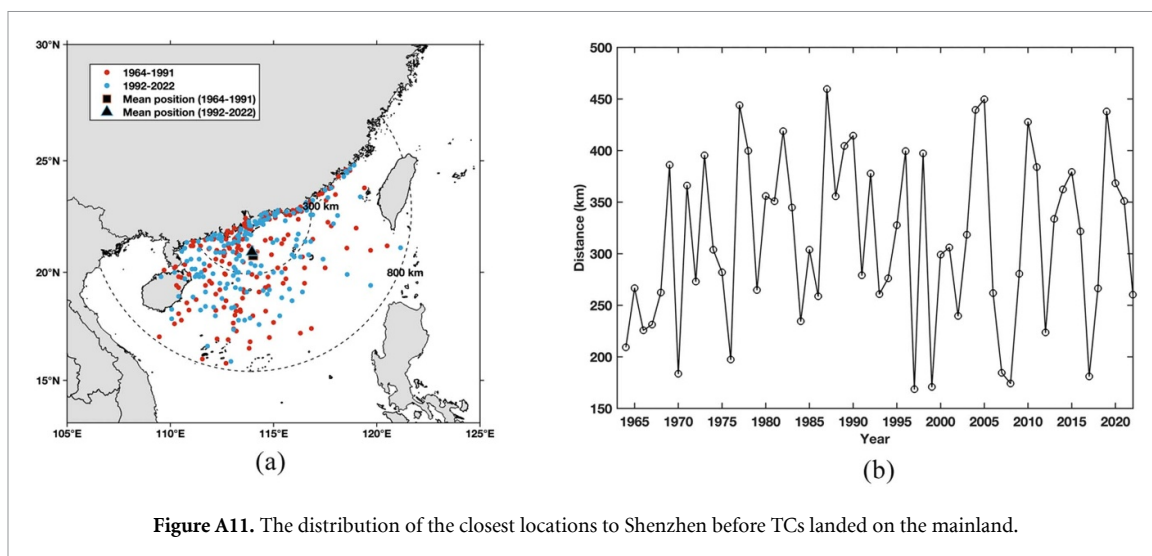
Figure A11. The distribution of the closest locations to Shenzhen before TCs landed on the mainland.
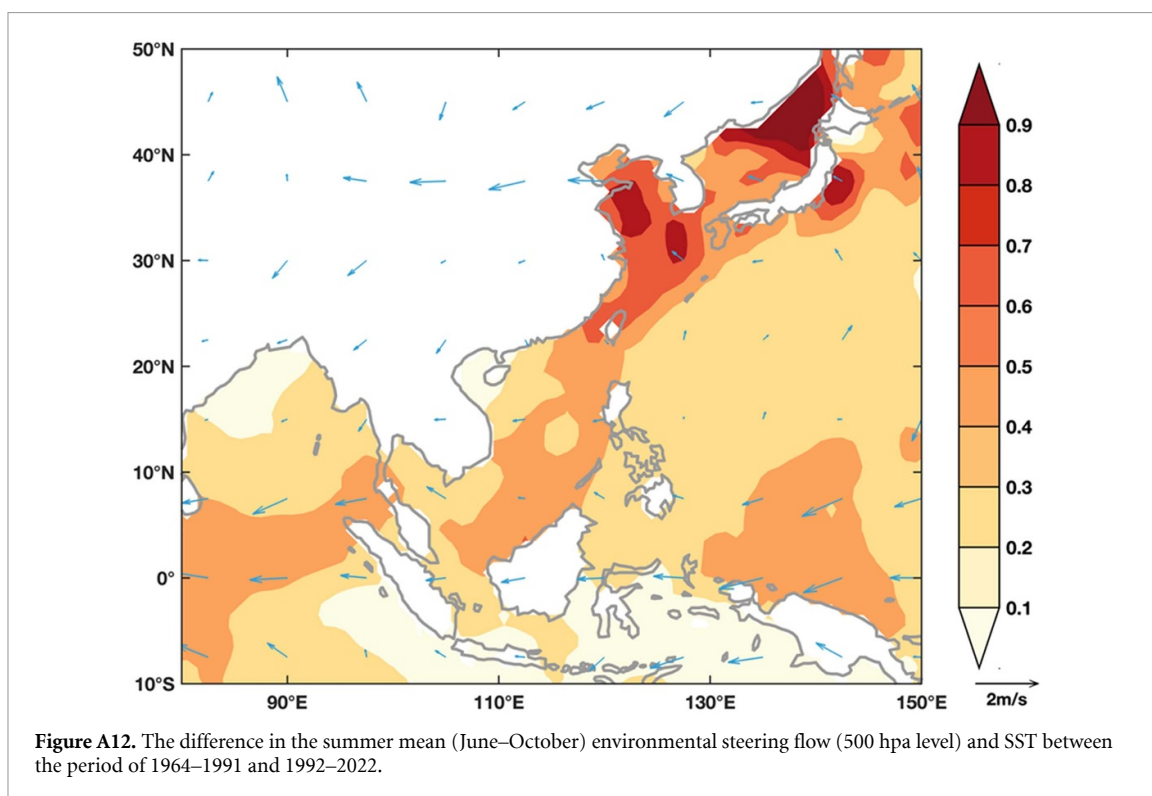

Figure A12. The difference in the summer mean (June–October) environmental steering flow (500 hpa level) and SST between the period of 1964–1991 and 1992–2022.

ORCID iDs

Andrew N Ross ⓘ https://orcid.org/0000-0002-8631-3512

Laixiang Sun ⓘ https://orcid.org/0000-0002-7784-7942

References

Barbier E B 2015 *Climate Change Impacts on Rural Poverty in Low-elevation Coastal Zones* (Policy Research Working Papers)

Chan Y K 1983 *Statistics of Extreme Sea-Levels in Hong Kong, Hong Kong Observatory* (Technical Note (Local))

Chang L, Liou J and Chang F 2022 Spatial-temporal flood inundation nowcasts by fusing machine learning methods and principal component analysis *J. Hydrol.* **612** 128086

Chen B 2014 *Why Urban "Drainage" Always Fails to Run the Storm* (Safety and Health)

Daloz A and Camargo S 2017 Is the poleward migration of tropical cyclone maximum intensity associated with a poleward migration of tropical cyclone genesis? *Clim. Dyn.* **50** 705–15

Du J 2020 *Shenzhen Experiment: The Story of China's Instant City* (Harvard University Press)

Gao C, Zhou L, Wang C, Lin I-I and Murtugudde R 2022 Unexpected limitation of tropical cyclone genesis by subsurface tropical central-north pacific during El Niño *Nat. Commun.* **13** 1

Hu P, Zhang Q, Shi P, Chen B and Fang J 2018 Flood-induced mortality across the globe: spatiotemporal pattern and influencing factors *Sci. Total Environ.* **643** 171–82

Huang Z, Zhang W, Wu H, Chen T, Fan J, Jiang P, Li Z and Huang B 2001 A prediction of sea level rising amplitude in 2030 and defensive countermeasures in the Zhujiang Delta *Sci. China D* **44** 446–54

IPCC 2021 Weather and Climate Extreme Events in a Changing Climate *Climate Change 2021: The Physical Science Basis* (Cambridge University Press) (https://doi.org/10.1017/9781009157896)

Joyce J, Chang N-B, Harji R, Ruppert T and Singhofen P 2017 Cascade impact of hurricane movement, storm tidal surge, sea level rise and precipitation variability on flood assessment in a coastal urban watershed *Clim. Dyn.* **51** 383–409

Ke Q, Tian X, Bricker J, Tian Z, Guan G, Cai H, Huang X, Yang H and Liu J 2020 Urban pluvial flooding prediction by machine learning approaches—a case study of Shenzhen city, China *Adv. Water Resour.* **145** 103719

Knutson T R, Chung M V, Vecchi G, Sun J, Hsieh T-L and Smith A J P 2021 Science Brief review: climate change is probably increasing the intensity of tropical cyclones *Critical Issues in Climate Change Science* ed C Le Quéré, P Liss and P Forste

Lee S, Kang T, Sun D and Park J 2020 Enhancing an analysis method of compound flooding in coastal areas by linking flow simulation models of coasts and watershed *Sustainability* **12** 6572

Lee S, L'Heureux M, Wittenberg A T, Seager R, O'Gorman P A and Johnson N C 2022 On the future zonal contrasts of equatorial pacific climate: perspectives from observations, simulations, and theories *npj Clim. Atmos. Sci.* **5** 1

Liu Q, Xu H and Wang J 2022 Assessing tropical cyclone compound flood risk using hydrodynamic modelling: a case study in Haikou City, China *Nat. Hazards Earth Syst. Sci.* **22** 665–75

Lu X Q, Yu H, Ying M, Zhao B K, Zhang S, Lin L M, Bai L N and Wan R J 2021 Western North Pacific tropical cyclone database created by the China meteorological administration *Adv. Atmos. Sci.* **38** 690–9

Ma P, Wang W, Zhang B, Wang J, Shi G, Huang G, Chen F, Jiang L and Lin H 2019 Remotely sensing large- and small-scale ground subsidence: a case study of the Guangdong–Hong Kong–Macao Greater Bay Area of China *Remote Sens. Environ.* **232** 111282

Mann H B 1945 Nonparametric tests against trend *Econometrica* **13** 245

Marsooli R, Lin N, Emanuel K and Feng K 2019 Climate change exacerbates hurricane flood hazards along US Atlantic and Gulf coasts in spatially varying patterns *Nat. Commun.* **10** 1

Ministry of Natural Resources 2023 Sea level bulletin of China 2022

Ng M K 2003 Shenzhen *Cities* **20** 429–41

Nicholls R J, Lincke D, Hinkel J, Brown S, Vafeidis A T, Meyssignac B, Hanson S E, Merkens J-L and Fang J 2021 A global analysis of subsidence, relative sea-level change and coastal flood exposure *Nat. Clim. Change* **11** 338–42

Nie Y, Tang C and Cheng Z 2016 *Projections of Maximum Sea Level Recurrence Interval near Shenzhen at the End of the 21th Century* vol 36 (Tropical Geography) pp 901–5

Peng J 1999 Causes and countermeasures of rainwater and sewage confluence in Shenzhen special economic zone *Water Wastewater Eng.* **25** 3 (in Chinese)

Qiang Y, Zhang L, He J, Xiao T, Huang H and Wang H 2021 Urban flood analysis for pearl river delta cities using an equivalent drainage method upon combined rainfall-high tide-storm surge events *J. Hydrol.* **597** 126293

Risk Warning for Major Meteorological Hazards in Shenzhen 2022 Retrieved 20 September 2022 (2022 Edition) Sz.gov.cn (available at: www.sz.gov.cn/cn/xxgk/zfxxgj/tzgg/content/post_9651695.html)

Sarica G, Zhu T, Jian W, Lo E and Pan T 2021 Spatio-temporal dynamics of flood exposure in Shenzhen from present to future *Environ. Plan.* B **48** 1011–24

Schmidt L, Heße F, Attinger S and Kumar R 2020 Challenges in applying machine learning models for hydrological inference: a case study for flooding events across germany *Water Resour. Res.* **56** 5

Shenzhen Climate Bulletin 2018 *Meteorological Bureau of Shenzhen Municipality Official Website* (available at: http://weather.sz.gov.cn/mobile/qixiangfuwu/qihoufuwu/qihouguanceyupinggu/nianduqihougongbao/content/post_3587622.html) (Accessed 11 November 2023)

Shenzhen flood control plan revision and river improvement plan: Revision report of flood control plan 2014–2020 (available at: http://swj.sz.gov.cn/attachment/0/783/783866/8100259.pdf) (Accessed 1 October 2023)

Song W, Tang S and Wang X 2019 Relationship between Pacific Ocean warming and tropical cyclone activity overthe western North Pacific *Stoch. Environ. Res. Risk Assess.* **33** 31–45

Sun J, Wang D, Hu X, Ling Z and Wang L 2019 Ongoing poleward migration of tropical cyclone occurrence over the Western North Pacific Ocean *Geophys. Res. Lett.* **46** 9110–7

Sun Y, Li T, Zhong Z, Yi L, Chen X, Ha Y, Zhu J, Shen Y, Xu Z and Hu Y 2018 A recent reversal in the poleward shift of Western North Pacific tropical cyclones *Geophys. Res. Lett.* **45** 9944–52

Wang C, Li C, Mu M and Duan W 2012a Seasonal modulations of different impacts of two types of ENSO events on tropical cyclone activity in the western North Pacific *Clim. Dyn.* **40** 2887–902

Wang H, Wright T J, Yu Y, Lin H, Jiang L, Li C and Qiu G 2012b Insar reveals coastal subsidence in the Pearl River Delta, China *Geophys. J. Int.* **191** 1119–28

Wang S and Toumi R 2021 Recent migration of tropical cyclones toward coasts *Science* **371** 514–7

Wang S and Toumi R 2022 On the intensity decay of tropical cyclones before landfall *Sci. Rep.* **12** 3288

Xing L, Huang L, Chi G, Yang L, Li C and Hou X 2018 A dynamic study of a karst spring based on wavelet analysis and the mann-kendall trend test *Water* **10** 698

Xinhua 2023 Extremely heavy rainstorm hits China's Shenzhen (available at: https://english.news.cn/20230908/5aedaf1da0a74e878e2d620d4976269d/c.html)

Yang Y, Yin J, Zhang W, Zhang Y, Lu Y, Liu Y, Xiao A, Wang Y and Song W 2021 Modeling of a compound flood induced by the levee breach at Qianbujing Creek, Shanghai, during Typhoon Fitow *Nat. Hazards Earth Syst. Sci.* **21** 3563–72

Ying M, Zhang W, Yu H, Lu X, Feng J, Fan Y, Zhu Y and Chen D 2014 An overview of the China meteorological administration tropical cyclone database *J. Atmos. Oceanic Technol.* **31** 287–301

Yu F J, Dong J X, Ye L, Hou J, Li M, Liu S and Fu C 2015 *Collection of storm surge disasters historical data in China 1949–2009* (China Ocean Press) in Chinese

Yu W, Zhang Y, Zhou W, Wang W and Tang R 2019 Urban expansion in Shenzhen since 1970s: a retrospect of change from a village to a megacity from the space *Phys. Chem. Earth* A/B/C **110** 21–30

Zhang Y and Najafi M R 2020 Probabilistic numerical modeling of compound flooding caused by tropical storm matthew over a data-scarce coastal environment *Water Resour. Res.* **56** 10

Zhang Z, Jian X, Chen Y, Huang Z, Liu J and Yang L 2023 Urban waterlogging prediction and risk analysis based on rainfall time series features: a case study of shenzhen *Front. Environ. Sci.* **11** 1131954

Zhou L, Wu X, Ji Z and Gao G 2017 Characteristic analysis of rainstorm-induced catastrophe and the countermeasures of flood hazard mitigation about Shenzhen city *Geomatics Nat. Hazards Risk* **8** 1886–97

Zou F, Tenzer R, Fok H S, Meng G and Zhao Q 2021 The sea-level changes in Hong Kong from tide-gauge records and remote sensing observations over the last seven decades *IEEE J. Sel. Top. Appl. Earth Obs. Remote Sens.* **14** 6777–91